ELSEVIER

Contents lists available at ScienceDirect

Journal of Catalysis

journal homepage: www.elsevier.com/locate/jcat



Structure and reactivity of single site Ti catalysts for propylene epoxidation



Zheng Lu^a, Xiaoyang Liu^c, Bin Zhang^d, Zhuoran Gan^a, Siwen Tang^{a,e}, Lu Ma^f, Tianpin Wu^f, George J. Nelson^b, Yong Qin^d, C. Heath Turner^c, Yu Lei^{a,*}

- ^a Department of Chemical and Materials Engineering, University of Alabama in Huntsville, AL 35899, USA
- ^b Department of Mechanical and Aerospace Engineering, University of Alabama in Huntsville, AL 35899, USA
- ^c Department of Chemical and Biological Engineering, University of Alabama, Tuscaloosa, AL 35487, USA
- d State Key Laboratory of Coal Conversion, Institute of Coal Chemistry, Chinese Academy of Sciences, Taiyuan 030001, China
- e Hunan Provincial Key Laboratory of Health Maintenance for Mechanical Equipment, Hunan University of Science and Technology, Xiangtan 411201, China
- ^fX-ray Science Division, Advanced Photon Sources, Argonne National Laboratory, Argonne, IL 60439, USA

ARTICLE INFO

Article history: Received 4 June 2019 Revised 25 July 2019 Accepted 26 July 2019

Keywords: Atomic layer deposition Single-atom catalysis Coordination number Titania Gold

ABSTRACT

Propylene epoxidation using molecular oxygen and hydrogen mixture on Au-based catalysts has attracted attention because of high propylene oxide selectivity and the use of an inexpensive and environmental friendly oxidant. Single-site titanium on metal oxide supports plays an important role in achieving high reactivity and selectivity in propylene epoxidation. Here we used TiO₂ atomic layer deposition (ALD) to synthesize single-site titanium imbedded in the SiO₂ framework for propylene epoxidation. High temperature calcination was used as post-treatment to control the titania structure and Ti—O coordination number. Using UV-vis spectroscopy and X-ray absorption spectroscopy, we successfully established that under similar propylene conversion the selectivity to propylene oxide (PO) is strongly correlated to the Ti—O coordination number and bond length. Using a cluster model, density functional theory (DFT) calculations indicate that the partial charges of single Ti—SiO₂ sites scale linearly as a function of the coordination number. Also, the predicted Ti—O bond lengths follow the same trend as found in the experiments, providing additional support for the observed experimental activity relationships.

© 2019 Elsevier Inc. All rights reserved.

1. Introduction

Propylene epoxidation using molecular oxygen is a promising, alternative route to synthesize propylene oxide (PO), a chemical of great industrial importance [1–5]. Since Haruta first discovered that supported gold nanoparticles on TiO₂ are active and selective for the direct epoxidation of propylene in the presence of molecular oxygen and hydrogen, it had been gradually realized that the reactivity, PO selectivity and hydrogen efficiency could benefit from synergic effects of small nano-sized gold particles and the neighboring TiO₂ [6] . Studies suggest that highly dispersed isolated Ti sites serve as the preferential sites to adsorb propylene, while the gold nanoparticles are responsible for the formation of the OOH* species from oxygen and hydrogen [7–9]. The OOH* species then migrate toward nearby Ti sites to produce PO from propylene. The isolation of Ti sites was found to increase the PO

selectivity with less byproduct formation. The adjacent Ti sites were found to favor bidentate adsorption of propylene, leading to the formation of undesired byproducts. Understanding the ${\rm TiO_2}$ structure is of great importance for designing highly efficient ${\rm Au-TiO_2}$ based catalysts for propylene epoxidation.

To establish the Ti structure and performance relationship, Haruta and coworkers deposited TiO₂ on non-porous silica using incipient wetness impregnation (IWI) and subsequently calcined the support up to 1000 °C [10]. The PO yield and selectivity improved by increasing the calcination temperature. The improved PO yield and selectivity were ascribed to the formation of the site-isolated tetrahedral TiO₂ in the SiO₂ framework with the presence of Ti—O—Si. However, as TiO₂ prepared by IWI tends to initially form clusters and nanoparticles on the SiO₂ support, it could be difficult to drive all of the TiO₂ to form single-site Ti in SiO₂ framework using high temperature calcination. Another potential concern is the possible loss of surface area due to the collapse of pores during high temperature calcination. Other efforts have been used to synthesize single-site catalysts for propylene epoxidation. To generate

^{*} Corresponding author. E-mail address: yu.lei@uah.edu (Y. Lei).

single-site Ti, Nijhuis and co-workers used a Ti-grafted silica method prepare Ti-doped SiO_2 for propylene epoxidation with H_2 and O_2 , and achieved promising activity with 2.7% propylene conversion and PO selectivity at 89.4% [11]. A sol-gel method was used to prepare site-isolated Fe in the SiO_2 framework for propylene epoxidation with O_2 , and showed good activity without the use of Au [12], however, the catalysts showed 33.6% PO selectivity at 5.5% conversion.

The establishment of the Ti structure and performance relationship can benefit from the use of uniformly dispersed single-site Ti on the SiO₂ support. In this study, we investigated the isolated TiO₂ single-site initially deposited on porous SiO2 by atomic layer deposition (ALD), a method that has been used to prepare single-site catalysts [13-15]. Advanced catalyst synthesis is advancing from obtaining understandings of the catalytic active sites [16] to assemble catalytic active architecture [17]. ALD represents a promising technique to construct catalytic active architecture in a "bottom-up" manner to achieve high activity, selectivity, and stability [18,19]. It is a thin film deposition technique that uses organometallic compounds as precursors. It enables conformal coatings because the deposition conditions are optimized to ensure the surface self-limiting reaction between the organometallic precursors and the reaction sites on the substrates. Under surface selflimiting reaction conditions, the gaseous organometallic precursor molecules, e.g., titanium isopropoxide or TTIP, preferentially react with the surface reaction sites, e.g., surface hydroxyl groups, forming stable intermediates on the substrate [20,21]. These stable, chemisorbed intermediates will not decompose to form TiO2 until a co-reactant is dosed, e.g., H₂O. The steric hindrance effect from the bulky TTIP ligands ensures that the intermediates distance from each other and prevent the possible formation of Ti-O-Ti bonds, and the chemisorption nature of the intermediates allows the facile formation of Ti-O-Si bonds. In a previous study, we have prepared site-isolated Ti for Au-based catalysts using TiO2 ALD for propylene epoxidation with H_2 and O_2 at $100 \,^{\circ}$ C [22]. The catalysts showed 90% selectivity at 100 °C, however the PO formation rate was relatively low, about 1-2 $g_{PO}\ h^{-1}\ kg^{-1}cat$. A substantial gain in PO formation rate and propylene conversion could be obtained by carrying out the reaction at higher reaction temperature. To maintain high PO selectivity at high temperature, it is necessary to optimize the catalyst structure that favors the PO formation pathway. In this work, we used ALD to generate singlesite Ti, followed by a post-ALD calcination to alter the coordination of Ti, and connect the Ti-O structure and its performance in propylene epoxidation with H₂ and O₂. Using ultraviolet–visible (UV–vis) diffuse reflectance spectroscopy and X-ray absorption spectroscopy (XAS), we investigated the structure of single-site Ti in the SiO₂ framework as a function of calcination temperature. The PO selectivity shows a linear correlation to the Ti—O coordination number and bond distance, and DFT calculations predict a linear scaling of the partial charge of the Ti site as a function of the coordination number and bond distance.

2. Experimental

2.1. Catalyst synthesis

 TiO_2 surface self-limiting reaction was performed in a low vacuum (\sim 1 Torr) atomic layer deposition (ALD) reactor (Gemstar-6, Arradiance). Ultrahigh purity N_2 (Airgas, 99.999%) was used as the carrier gas and further purified using a Supelco gas purifier (Sigma-Aldrich) before entering the reactor. In a typical preparation, 0.5 g of SiO_2 (Silicycle S10040M) was uniformly spread onto a stainless steel tray held at $200\,^{\circ}$ C. Titanium isopropoxide (TTIP) was used as the precursor and contained in a stainless steel bub-

bler held at 75 °C to generate sufficient vapor pressure for deposition. The TTIP vapor was introduced to SiO_2 by N_2 carrier gas for 25 sec to 350 sec. The ALD reactor was then evacuated for 200 sec before introducing water vapor for 45 sec. The as-prepared support is named Ti— SiO_2 _ALD.

The quantity of TiO_2 deposited on the SiO_2 was determined by direct weight measurement performed before and after the deposition with a precision of 0.1 mg. The as-prepared $Ti-SiO_2$ then underwent calcination at 400, 600, 800, and $1000\,^{\circ}C$ for 2 h, respectively, as post-treatment. The post-treated supports were denoted as $Ti-SiO_2$ _ALD400, $Ti-SiO_2$ _ALD600, $Ti-SiO_2$ _ALD800, and $Ti-SiO_2$ _ALD1000.

Incipient wetness impregnation (IWI) of a methanol solution of titanyl acetylacetonate (TAA) was used to deposit TiO_2 on SiO_2 , following the recipe from Haruta's group [10]. After the impregnation (0.9 ml solution for 1 g of SiO_2), the methanol solvent was removed at 50 °C in a vacuum oven and dried at 70 °C for 4 h. The nominal TiO_2 loading was 1.3 wt%. The as-prepared $Ti-SiO_2$ _IWI was subsequently calcined at 800 °C and denoted as $Ti-SiO_2$ _IWI800.

Deposition of gold on Ti—SiO $_2$ supports was carried out using deposition precipitation (DP). Approximately 0.2 g of HAuCl $_4$ ·3H $_2$ O (Sigma Aldrich, 99.99%) was added to 100 ml of deionized water, followed by addition of 1 g of Ti—SiO $_2$. NaOH (1 mol/L) was dropwise added to the solution to keep the pH at \sim 7 for 2 h. The solid was separated from the solution, washed by 50 ml deionized water, separated again, and finally dried under vacuum at room temperature overnight.

2.2. Catalyst characterization

The high angle annular dark field scanning transmission electron microscopy (HAADF-STEM) imaging was performed using an FEI Tecnai F-20 transmission electron microscope equipped with a 200 keV thermal Schottky Field emission gun. The size histogram of gold nanoparticles was determined by measuring the diameter of more than 250 particles for each catalyst. UV-Vis absorption spectra were obtained on a Thermo Scientific Evolution 220 spectrophotometer fitted with an integrating sphere. Reflectance measurements were performed on powdered samples using a standard barium sulphate powder as a reference. X-ray diffraction (XRD) measurement was carried out using a Rigaku MiniFlex 600 powder X-ray diffractometer using Cu K-alpha radiation operated at 40 kV and 15 mA; 2 theta data from 2° to 90° were obtained at a scanning speed of 0.5°/min. Fourier transform infrared (FTIR) spectroscopy measurements were performed on a Bruker TENSOR27 spectrometer with the samples pre-pressed with KBr into pellets. Inductively coupled plasma mass spectroscopy (ICP-MS) analysis was performed using Agilent 7700x equipped with an ASX 500 autosampler. The system was operated at a radio frequency power of 1550 W and elements were measured in kinetic energy discrimination (KED) mode. Nitrogen adsorption-desorption experiments were carried out on a gas sorption analyzer (Autosorb iQ, Quantachrome Instruments) at 77 K. In a typical experiment, the sample was outgassed at 623 K for 10 h. The specific surface area was calculated using the Brunauer-Emmett-Teller (BET) method and the pore volume and size were obtained by the Barrett-Joyner-Halenda (BJH) method. The in situ quartz crystal microbalance (QCM) measurements were carried out in real time during TiO₂ ALD, typically at 200 °C. The time sequence for operating one ALD cycle of TiO_2 during the QCM measurements is 1-5-1-5 s. The Maxtek BSH-150 bakeable sensor with an AT-cut quartz sensor crystal was housed in the center of the ALD chamber. A Maxtek TM 400 film thickness monitor was used to record the mass gain during the TiO₂ ALD process. X-ray absorption spectroscopy (XAS) measurements, including extended X-ray absorption fine structure spectroscopy (EXAFS) and X-ray absorption near edge structure spectroscopy (XANES), were conducted at the Ti K edge (\sim 4966.4 eV) at beamline 9-BM at Advanced Photon Source (APS) at Argonne National Laboratory. The XAS spectra were recorded in fluorescence mode. EXAFS regime data fittings were performed using Artemis in the IFEFFIT software package. A single shell model fit of the EXAFS data was obtained between k = 3.0–12.0 Å $^{-1}$ and r = 1–2 Å, respectively.

2.3. Catalyst evaluation

Approximately 0.15 g catalyst of 60-80 mesh size, dilute with 1.5 g quartz sand of 25-35 mesh size, was used for gas-phase propylene epoxidation. The reaction was carried out in a quartz tubular reactor with a diameter of 10 mm under normal pressure. A blank experiment was performed under reaction conditions using only the quartz sand. A thermocouple was attached on the quartz tube wall where the catalyst was located to directly measure the reaction temperature. The reactant mixture consisted of 10 vol% each of hydrogen (Airgas, 99.999%), oxygen (Airgas, 99.999%), propylene (Matheson, 99.9%), and carried in 70 vol% argon (Airgas, 99.999%) with a total flow of 35 ml/min, equivalent to a gas hourly space velocity (GHSV) of 14,000 ml h^{-1} g_{cat}^{-1} . Without any pretreatment of the catalyst, the reaction temperature was reached by using a ramping rate of 1.5 K/min to 200 °C. The effluent gas line was heated to above 80 °C to prevent condensation of all the byproducts. The catalytic performance represents average data values after the performance stabilized.

The concentration of the reactants and products was measured online by two gas chromatographs, SRI 8610C equipped with a thermal conductivity detector (TCD) and Agilent 5890 equipped with a flame ionization detector (FID). Oxygen, hydrogen, CO₂, and propylene were separated using a molecular sieve column and analyzed via TCD, while propylene oxide, ethanal, propanal, acetone, and acrolein were separated using a RT-U-BOND column and analyzed via FID. The propylene conversion and product selectivity were described previously [22]. H₂ efficiency was calculated as moles of PO/moles of H₂ converted. Turnover frequencies (TOFs) were calculated based on the number of surface Au atoms.

3. Results and discussion

3.1. Experimental analysis

The SiO₂ gel support (Silicycle S10040M) used in this work has a specific surface area of 93.3 m²/g. Assuming a growth rate of 0.3 Å/cycle and TiO₂ density of 4.23 g/cm³ [22], the volume of TiO₂ deposited on 1 g of the support after one ALD cycle equals to 93.3 m² times 0.3 Å. Thus, the expected weight gain on 0.5 g of SiO_2 after one ALD cycle of TiO_2 is ~ 1.3 wt%. Weight gain measurements were performed to establish the appropriate exposure conditions to saturate the SiO₂ surface and ensure that the deposition was surface reaction controlled in the reactor. Fig. 1 shows the results of weight-gain measurements performed on 0.5 g SiO₂ sample after coating with one cycle of TiO2 ALD using the timing sequence x-200-45-200 sec. The TTIP exposure time x was altered between 0 and 350 sec. The weight gain increases with TTIP exposure time up to a duration of \sim 250 sec, after which the weight gain remains a constant at \sim 1.4 wt%. The saturated weight gain is confirmed by ICP measurement which shows the TiO2 loading is \sim 1.3 wt%. This is within the error of weight gain experiments and the expected weight gain, based on the growth rate of 0.3 Å/cycle.

After one ALD cycle of TiO_2 was deposited on SiO_2 gel at 200 °C, the as-prepared TiO_2/SiO_2 supports were subsequently calcined to 400 °C, 600 °C, 800 °C, and 1000 °C for 2 h. The XRD patterns in

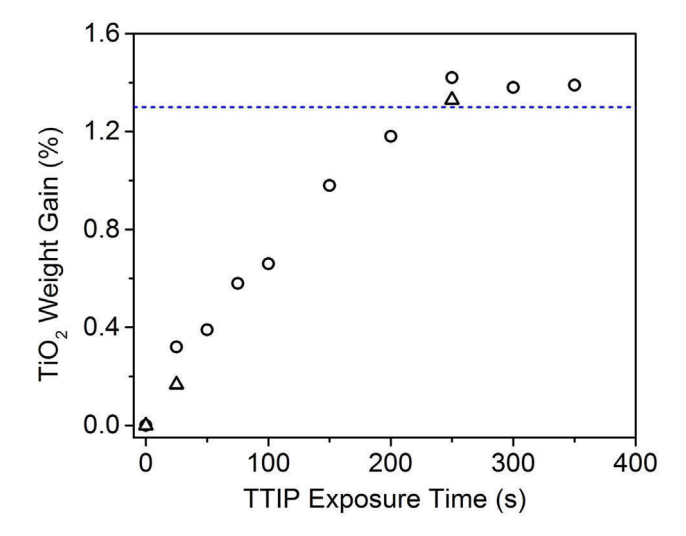


Fig. 1. Measurements of TiO_2 ALD saturation versus TTIP exposure time performed on SiO_2 obtained from weight-gain measurements (circles) and ICP measurements (triangles). The dashed line indicates the expected weight gain based on 0.3 Å/cycle [22] determined by QCM measurement.

Fig. 2a show no peaks for TiO_2 , except a broad feature at 2θ between 20° and 30° that is representative of amorphous SiO_2 . The lack of TiO_2 features in XRD patterns suggests that there is no large, crystalline TiO_2 on the SiO_2 surface.

The detailed IR spectra are presented in Fig. 2b. The peaks at about 475, 810, 1110 and 1210 cm⁻¹ are due to the stretching of Si-O-Si [23]. The absence of a Ti-O-Ti feature at 1400 cm⁻¹ indicates that the Ti sites are isolated by SiO₂, which is consistent with the XRD results [24,25]. The band at about 965 cm⁻¹ is assigned to the characteristic bond vibration of Ti-O-Si [10,26]. This result showed that the interaction of TiO₂ with silica gel existed even without calcination. Haruta and coworkers synthesized Ti-SiO₂ using titanyl acetylacetonate (TAA) as the precursor. The feature at 965 cm⁻¹ was not observed until the sample was calcined at 1000 °C and the Ti gradually embedded into SiO2 the framework to generate Ti-O-Si interactions at high temperature [10]. In a study by Wachs and coworkers, Ti-SiO₂ was prepared by IWI with TTIP as the precursor and a similar phenomenon was observed, except that the Ti-O-Si feature appeared at a lower calcination temperature [27]. The Ti-O-Si feature in the as-prepared Ti-SiO₂ ALD suggested that the bridge Ti-O-Si was established during the TiO₂ ALD process.

Rahtu and Ritala carried out a combined quartz crystal microbalance (QCM) and quadrupole mass spectrometry (QMS) study of TiO2 ALD and suggested that the TTIP precursor reacts with the surface —OH group, as illustrated in equation (1), which leads to the formation of the bridge Ti-O-Si and a thermally stable intermediate $-Ti(OCH(CH_3)_2)_3$ [28]. In the subsequent water exposure in TiO₂ ALD shown in equation (2), the intermediate $-Ti(OCH(CH_3)_2)_3$ becomes a metastable species $-Ti(OH)_3$ which quickly interacts with surface hydroxyl groups, forming a threefold bonded $(Si - O -)_3 TiOH$ as shown in equation (3). Reaction (2) and (3) could occur simultaneously. The density of the surface hydroxyl groups is estimated to be about 4.9 OH groups per nm² [29]. Theoretically, if each surface hydroxyl group can anchor one Ti, the maximal amount of TiO₂ can be deposited is about 6.1 wt % on the SiO_2 with the surface area about 93.3 m²/g. The IR spectroscopy of the ALD Ti-SiO₂ suggests that the steric hinderance effect of the bulky $(OCH(CH_3)_2)_3$ ligands successfully prevented the formation of oligomeric TiO2, leading to the formation of site-isolated Ti with a TiO₂ loading of about 1.3 wt%.

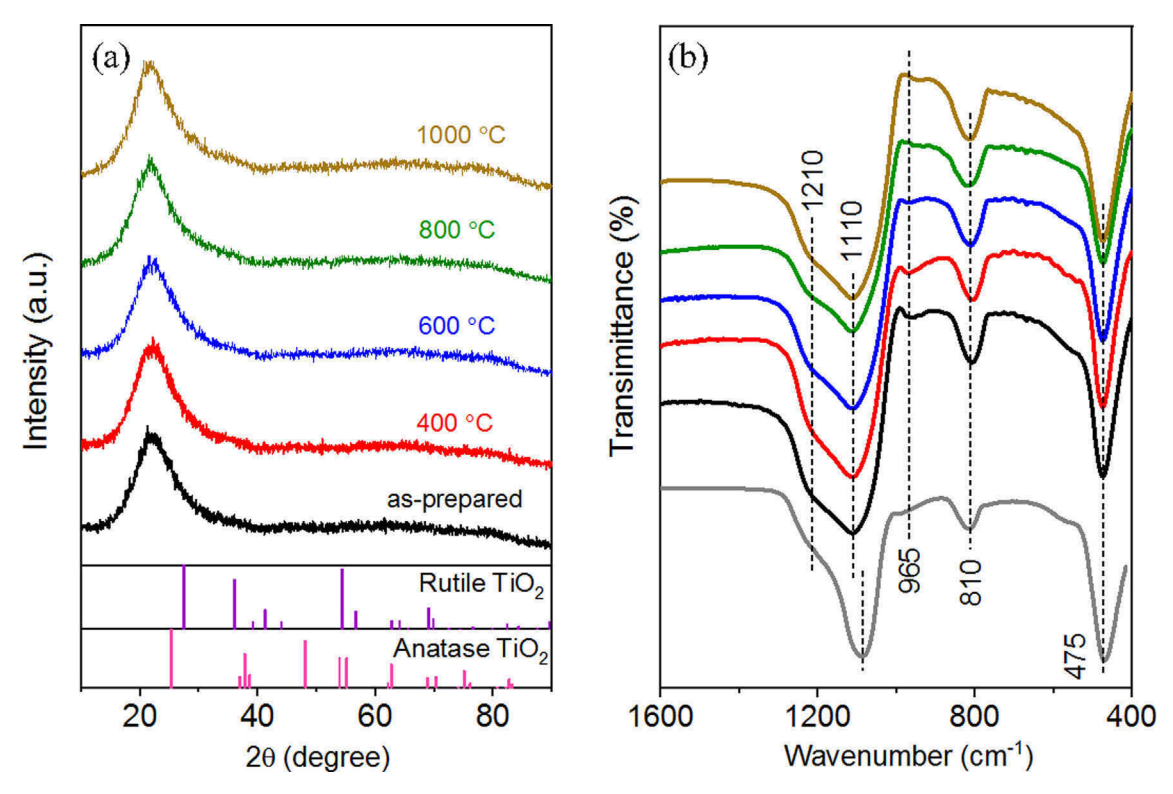


Fig. 2. (a) XRD patterns and (b) IR spectra of the Ti—SiO₂_ALD samples. Gray – SiO₂ support; black – as-prepared Ti—SiO₂_ALD; red – Ti—SiO₂_ALD400; blue – Ti—SiO₂_ALD400; blue – Ti—SiO₂_ALD400; green – Ti—SiO₂_ALD800, dark yellow – Ti—SiO₂_ALD1000.

$$Si - OH(s) + Ti(OCH(CH_3)_2)_4(g)$$

$$\rightarrow Si - O - Ti(OCH(CH_3)_2)_2(s) + (CH_3)_2CHOH(g)$$
(1)

$$Si - O - Ti(OCH(CH_3)_2)_3 + 3H_2O$$

 $\rightarrow Si - O - Ti(OH)_3(s) + 3(CH_3)_2CHOH(g)$ (2)

$$2Si - OH(s) + Si - O - Ti(OH)_3(s)$$

$$\rightarrow (Si - O-)_3 TiOH(s) + 2H_2O(g)$$
(3)

Here we need to point out that the Ti—O coordination number of the ALD TiO $_2$ cannot be simply assigned to four since the change in hybridization geometry is not taken into consideration. The precursor TTIP has four $OCH(CH_3)_2$ ligands surrounding the Ti $^{4+}$. The valence electrons configuration for Ti $^{4+}$ in TTIP is [Ne] $3s^23p^34s^13d^2$. The electrons from the $(OCH(CH_3)_2)_3$ ligands filled into the orbitals of $3p^34s^1$, this sp 3 hybridization shows that the TTIP molecule has a tetrahedron structure. The $(OCH(CH_3)_2)_3$ ligands replaced by oxygen after 1 cycle of TiO $_2$ ALD, the electrons from the oxygen filled into the orbitals of $3p^34s^13d^2$, this sp $^3d^2$ hybridization indicates the formation of octahedron structure.

The UV–vis spectra in Fig. 3a show that with increasing calcination temperature, the spectra appearing between 220 and 340 nm, which is attributed to incorporated Ti⁴⁺, become narrower (blueshift). Similar phenomenon was observed in Fig. S1 which shows the UV–vis absorption spectra of the Ti–SiO₂_IWI samples after 800 °C calcination. It is evident that the Ti coordination number decreased with increasing calcination temperature as the ligand to metal charge transfer (LMCT) band for octahedral Ti sites is expected to be at a higher wavelength than the tetrahedral Ti sites [30,31].

Fig. 3b shows the BET surface area and pore volume of the Ti— SiO_2 _ALD samples. The corresponding N_2 adsorption-desorption isotherms are shown in Fig. S2. Table S1 summarizes

the surface area, pore volume, and pore diameter of the Ti-SiO₂ samples. The SiO₂ has an average surface area of 93 m²/g and pore volume of 0.949 cm³/g. Elam deposited up to 20 ALD cycles of Al₂O₃ on the same SiO₂ without observing change of surface area. [32] In our case, one ALD cycle of TiO₂ did not alter the surface area, pore volume, or pore diameter. The surface area of the support decreased after calcination. It became 90 m²/g after 800 °C calcination but dramatically decreased to 55 m²/g after 1000 °C calcination. The pore volume of the Ti-SiO₂_ALD samples as a function of calcination temperature appeared to follow the same trend as the BET surface area. The pore diameter of the samples remained at about 29 ± 1.6 nm for all samples. The decrease in BET surface area was probably due to the collapse of the pore openings of the SiO₂ support, restricting the accessibility of reactants to surface active sites. The corresponding N2 adsorption-desorption isotherms of the Ti—SiO₂_IWI samples are shown in Fig. S3. The pore volume and pore diameter of the Ti-SiO2_IWI support are 0.558 cm³/g and 20.7 nm, respectively, significantly smaller than the pristine SiO₂. The After 800 °C calcination, the surface area of Ti-SiO₂ decreased from 101 m²/g to 88 m²/g without significant changes in pore volume or pore diameter.

X-ray absorption near edge spectroscopy (XANES) and extended X-ray absorption near edge structure (EXAFS) have been developed as reliable tools in the investigation of the coordination geometry of Ti atoms in the SiO_2 matrix [33,34]. The pre-edge features of XANES can also provide information about the coordination geometry of Ti^{4+} cations. Ti^{4+} is in a d^0 configuration corresponding to the A_1 state in tetrahedral symmetry and A_{1g} state in octahedral symmetry. Due to the presence of an inversion center at Ti sites in octahedral symmetry, the transitions from A_{1g} to T_{2g} and T_{2g} and T_{2g} to T_{2g} to T_{2g} to T_{2g} and T_{2g} to T_{2g}

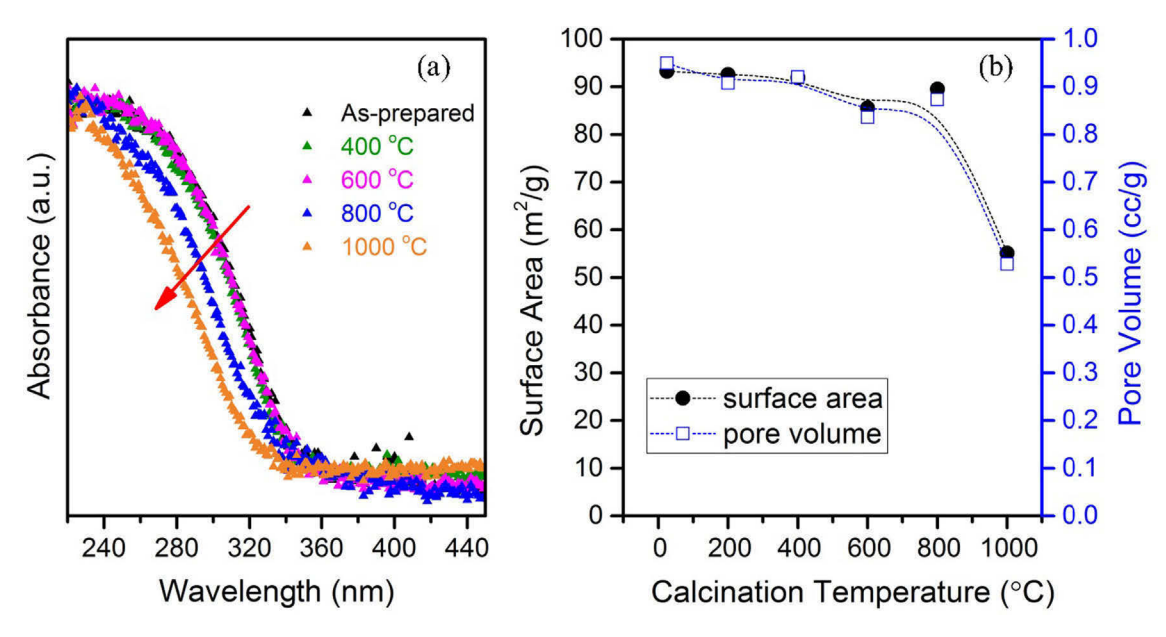


Fig. 3. (a) UV-Vis spectra and (b) BET surface area and pore volume of Ti-SiO₂_ALD samples. The arrow indicates increasing calcination temperature.

However, only considering the absorption peak intensity may lead to overestimation of the Ti coordination number. The pre-edge energy position is another indicator of the Ti coordination number [36]. Using both parameters is an effective way to estimate the Ti coordination number especially when mixtures of different Ti coordination exist. In general, the overall Ti coordination number decreased accompanied by a decrease in pre-edge energy, with a corresponding increase in normalized peak intensity.

Fig. 4a and 4b show the pre-edge region of the Ti K-edge XANES spectra for the supports prepared using ALD and IWI, respectively. Particularly, the pre-edge energy at ~4970 eV shifted to a lower photon energy level with increasing calcination temperature. Regardless of the preparation methods, Fig. 4c shows that the normalized pre-edge intensity inversely relates to the pre-edge energy, which demonstrated that the overall Ti coordination number decreased after calcination, consistent with the UV-vis spectra. However, it is not plausible to determine if the Ti⁴⁺ is exclusively in one coordination state or in a mixture of different Ti coordination states from only the XANES analysis.

Fig. 5a and b illustrate the Fourier transformation (FT) of EXAFS spectra of Ti—SiO₂_ALD and Ti—SiO₂_IWI samples, respectively. As compared with the EXAFS spectra of TS-1 and TiO₂ P25 shown in Fig. 5c, the most significant peak at an un-corrected distance of about 1.5 Å corresponds to the first shell of the Ti—O path. The peak intensity increases with increasing calcination temperature. The peak at the un-corrected distance of about 2.7 Å is assigned to the long range Ti—O—Ti path which could be an indicator of the presence of adjacent Ti sites. The Ti—O—Ti peak intensity of the EXAFS spectra of the Ti—SiO₂_ALD and Ti—SiO₂_IWI samplesare close to the noise level, probably due to small or no population of adjacent Ti sites, which explains the lack of any TiO₂ domains in the XRD patterns.

The detailed EXAFS data fitting to the Ti—SiO₂ samples are listed in Table 1. The as-prepared Ti—SiO₂—ALD has an average Ti—O first shell coordination of 5.4, indicating a possible mixture of 5-fold and 6-fold coordinated Ti sites. The Ti—O first shell coordination number decreases from 5.4 to 4.0 with increasing calcination temperature from 400 °C to 1000 °C. Note that a coordination number

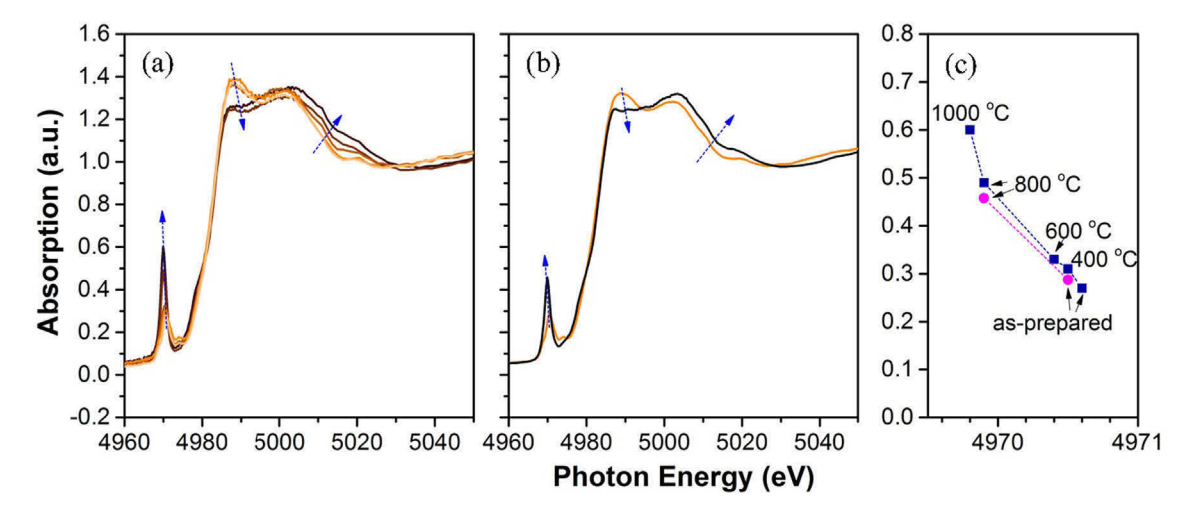


Fig. 4. Pre-edge region of Ti K-edge XANES spectra of (a) Ti—SiO₂_ALD samples and (b) Ti—SiO₂_IWI samples. The arrows indicate the increase in calcination temperature. (c) Pre-edge position vs the intensity (blue – Ti—SiO₂_ALD samples, pink – Ti—SiO₂_IWI samples).

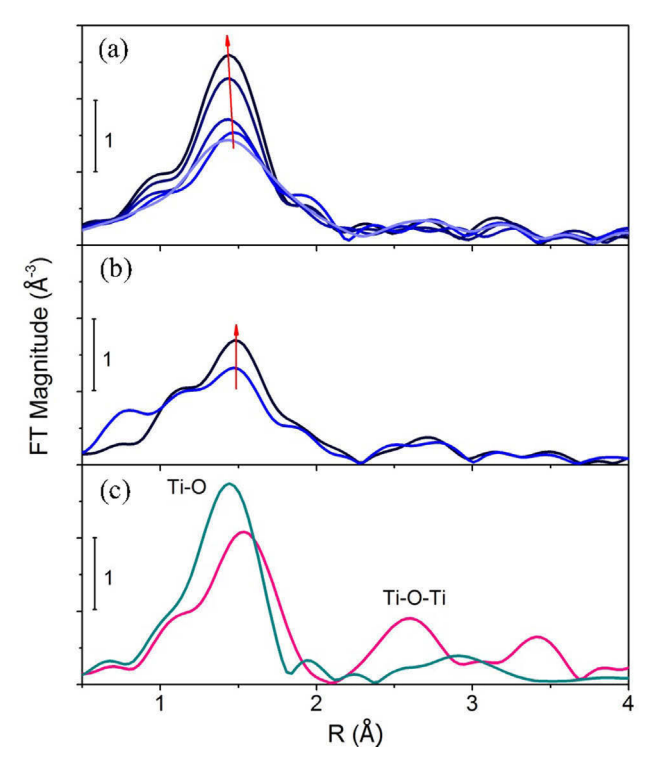


Fig. 5. Ti K-edge EXAFS Fourier transform data for the (a) Ti— SiO_2 _ALD samples, (b) Ti— SiO_2 _IWI samples, and (c) reference compounds. The arrows in (a) and (b) indicate increasing calcination temperature. *Olive* – TS-1, *Red* – TiO_2 P25.

4.0 is expected for the four-fold, isolated Ti site in TS-1. At the same time, the Ti—O bond distance showed slight bond contraction from 1.86 Å to 1.82 Å. The Ti-O coordination number and bond distance in Ti-SiO₂ _ALD800 and Ti-SiO₂ _ALD1000 are similar to those in titanium silicalite-1 (TS-1). As compared with the as-prepared Ti-SiO₂_ALD sample, the Ti-O coordination number of the asprepared Ti—SiO₂_IWI sample is 6.2, close to the Ti—O coordination number of the TiO₂ P25 reference, which is known to lead to CO₂ formation in propylene epoxidation. After being calcined at 800 °C, the first shell coordination number of the Ti-SiO₂_IWI800 sample decreased to 4.9, higher than the CN in Ti-SiO₂_ALD800. One possible explanation is that the ALD samples are mostly site-isolated Ti and can be easily embedded into the SiO2 framework using high temperature calcination. The IWI samples contain a discernible amount of agglomerated TiO₂ which is too small to be detected by XRD and second shell Ti-O-Ti in EXAFS, but the agglomerated TiO₂ makes it difficult to generate 4-coordinated, site-isolated Ti sites.

Gold nanoparticles are deposited on a series of Ti—SiO₂ samples using deposition precipitation (DP). ICP-MS measurements showed that the loading of gold was \sim 0.03 wt%. Fig. 6 shows that the gold nanoparticles are homogeneously dispersed on the Ti-SiO2_ALD support. The bright dots are gold nanoparticles with an average diameter of 2.4 ± 0.6 nm. Additional STEM images of Au/Ti-SiO₂-ALD800 in Fig. S4 showed Au with similar particle size of 2.4 nm. The diameter of gold nanoparticle is expected to closely related to its loading, preparation temperature, pH, and the Ti:Si in the support [37]. The gold nanoparticles in this work were prepared under the same conditions using DP and the Ti:Si were identical in all samples. Therefore, 2.4 nm was used to calculate the TOFs. Although the presence of site-isolated Ti was identified by FT-IR, UV-vis, and XAS spectra, it is difficulty to identify Ti using STEM due to its relative low atomic number (z = 22) and its low loading $(\sim 1.3 \text{ wt\% or } \sim 1 \text{ mol\%}).$

Fig. 7 and Table 2 summarize the performance of Ti-SiO₂ supported gold catalysts in propylene epoxidation. All the catalysts were evaluated at close to 1% conversion to ensure that the system is a differential reactor. Major product propylene oxide and byproducts including ethanal, acrolein, propanal, and acetone were detected and quantified. Haruta found that propane could be produced in propylene epoxidation when Au nanoparticles were smaller than 2 nm as small Au nanoparticles favor hydrogenation pathway [38]. Formation of propane was not observed in any of our experiments as the Au nanoparticles were larger than 2 nm. As the Ti-O coordination number decreases from 5.4 in Au/ Ti-SiO₂_ALD to 4.1 in Au/Ti-SiO₂_ALD800, the selectivity to PO increases from 54% to 85%. The Au/Ti-SiO2_ALD800 catalyst showed the highest selectivity to PO, PO formation rate, and hydrogen efficiency. It has a PO formation rate was 24.2 gPO h^{-1} kg_{cat}⁻¹ or 417.2 mmolPO h^{-1} g_{cat}^{-1} , and a TOF of 0.11 s^{-1} . The high performance of Au/Ti-SiO₂_ALD800 catalyst can be ascribed to the presence of 4coordinated Ti single sites on SiO₂. The 5-fold and 6-fold coordinated Ti single sites could still lead to the formation of CO2 and other organic byproducts, as evidenced by the performance of Au/ Ti-SiO₂_ALD and Au/Ti-SiO₂_ALD600. Au/Ti-SiO₂_ALD1000 also showed high PO selectivity but lower propylene conversion due to the loss of about 40% SiO2 surface area after 1000 °C calcination, leading to a reduced amount of Ti and gold active sites.

Similarly, the performance of Ti—SiO₂_IWI800 was higher than Ti—SiO₂_IWI in terms of PO selectivity and PO formation, which again demonstrated the important impact of low coordination Ti species in propylene epoxidation. The Au/Ti—SiO₂_IWI800 catalyst showed a formation rate of 343.1 mmolPO h⁻¹ kg⁻¹ and a TOF of 0.09 s⁻¹. The propylene conversion and PO selectivity at 200 °C were 0.9% and 62%, respectively. Haruta and co-workers prepared a series of Au/Ti—SiO₂ catalyst combining a similar IWI method and post-synthesis calcination. The catalysts were examined in propylene epoxidation with H₂ and O₂ up to 150 °C [10]. They observed

Table 1 EXAFS fit parameters (k^2 : $\Delta k = 3.0-12 \text{ Å}^{-1}$ and $\Delta r = 1-2 \text{ Å}$).

Samples	Shell	CN ^a	R(Å) ^b	$\sigma^2(\mathring{A}^2)$	ΔE_0 (eV)
TiO ₂ P25	Ti—O	6	1.95	0.002	9.8
	Ti—O—Ti	4	3.00	0.002	0.8
TS-1	Ti—O	4	1.82	0.0005	8.5
Ti-SiO ₂ _ALD	Ti—O	5.4	1.86	0.009	3.4
Ti-SiO ₂ _ALD400	Ti—O	4.9	1.87	0.008	4.4
Ti-SiO ₂ _ALD600	Ti—O	4.5	1.84	0.006	4.3
Ti-SiO ₂ _ALD800	Ti—O	4.1	1.82	0.002	6.7
Ti-SiO2_ALD1000	Ti—O	4.0	1.82	0.002	8.6
Ti-SiO ₂ _IWI	Ti—O	6.2	1.86	0.011	2.8
Ti-SiO ₂ _IWI800	Ti-O	4.9	1.86	0.006	8.0

^a CN-Coordination number.

^b R-average bond distance. The values in italics have been fixed.

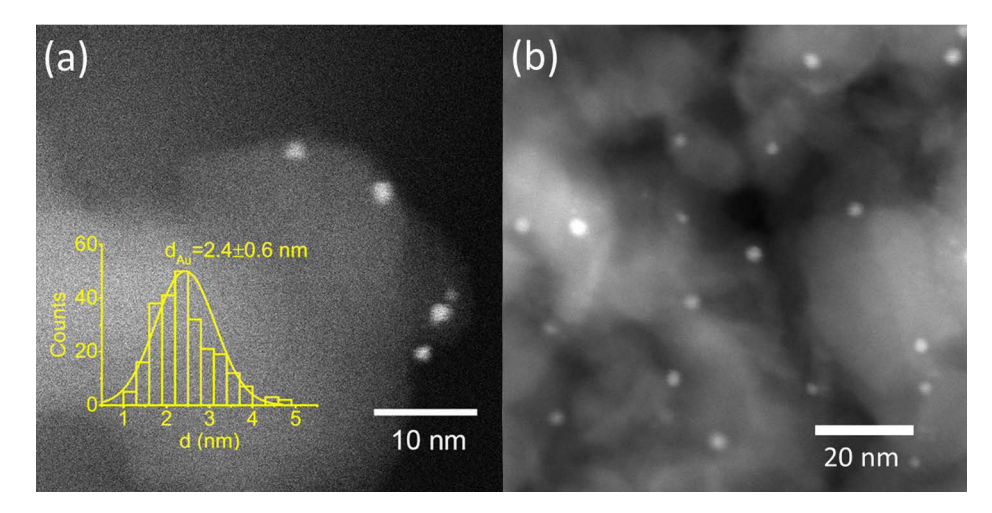


Fig. 6. STEM images for Au/Ti-SiO₂_ALD. The inset shows the Au nanoparticle size distribution.

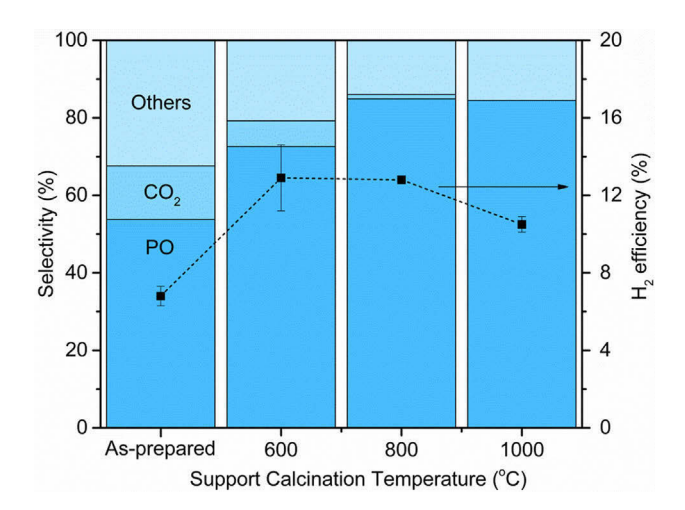


Fig. 7. Product selectivity and H_2 efficiency as a function of support calcination temperature. ("others" contains ethanal, acrolein, propanal, and acetone). Reaction conditions: reaction temperature 200 °C, $H_2/C_3H_6/O_2/N_2 = 3.5/3.5/3.5/24.5$ ml min⁻¹, space velocity = 14,000 ml h⁻¹ g_{cat}^{-1} .

increasing catalyst performance with increasing calcination temperature. The best catalyst was calcined at $1000\,^{\circ}\text{C}$ which showed 0.43%

propylene conversion and 56% PO selectivity at 150 °C. The PO selectivities of Au/Ti—SiO $_2$ -IWI catalysts in this work and Haruta's early work were lower than the ALD catalysts, which was probably due to the presence of adjacent Ti—O—Ti sites in the IWI catalysts, leading to significant CO $_2$ formation.

Table S2 compared the catalytic properties of the Au-based catalysts for propylene epoxidation with H_2 and O_2 . Ti containing SiO_2 framework such as TiO_2 modified SiO_2 , [7,10,11] Ti-TUD, [39] Ti-MCM-41, [40] and TS-1[7,37,41-47] were studied as the support materials. Au/TS-1 catalysts showed the highest PO formation rate and TOFs. For example, Lee reported PO formation rate of ~ 160 gPO·h $^{-1}$ ·kg $^{-1}_{cat}$ or ~ 2759 mmolPO h $^{-1}$ kg $^{-1}_{cat}$ at 200 °C [37]. The PO formation rate normalized to the total catalysts mass can be affected by several factors, including gold loading, dispersion, mass of catalyst used, reaction temperature, reaction feedstock space velocity, etc. TOFs reflects the intrinsic kinetic of the catalysts. [48,49] The highest TOF in propylene epoxidation with H_2 and O_2 was reported on Cspromoted Au/TS-1 catalyst whose TOF was 0.2 s $^{-1}$. The Au/Ti—SiO $_2$ -ALD800 catalyst exhibited a comparable TOF of 0.11 s $^{-1}$, owing to the controlled presence of site-isolated, 4-fold coordinated Ti.

Previous studies have shown that low coordinated Ti sites favor high PO selectivity [37,50]. For example, Oyama and coworkers investigated the coverage of OOH* species on Ti sites from Au-Ba/Ti-TUD catalysts, based on X-ray absorption spectroscopy (XAS) measurements. They found that the coverage of OOH* spe-

Table 2Performance of all the catalysts investigated.

#	C ₃ H ₆ conv (%)	Selectivity (%)					PO rate ^a	PO rateb	TOF [€]	H ₂ efficiency (%)	
		PO	Et	Ac	Pr	Ace	CO ₂				
1	0.7 ± 0.0	53.8 ± 1.9	6.2 ± 0.5	6.0 ± 1.3	15.1 ± 3.1	5.1 ± 0.9	13.8 ± 4.3	13.1	225.9	0.06	6.8
2	0.9 ± 0.1	72.6 ± 0.8	3.5 ± 0.6	6.1 ± 0.6	8.6 ± 0.4	2.6 ± 0.3	6.6 ± 0.8	21.5	370.7	0.10	12.9
3	0.8 ± 0.0	84.9 ± 0.3	2.1 ± 1.0	4.8 ± 0.2	5.3 ± 0.3	1.8 ± 0.1	1.1 ± 0.1	24.2	417.2	0.11	12.8
4	0.5 ± 0.0	84.5 ± 0.3	1.5 ± 0.1	7.9 ± 0.1	4.4 ± 0.2	1.6 ± 0.1	0.0 ± 0.0	12.3	212.1	0.05	10.5
5	0.8 ± 0.0	35.8 ± 0.1	6.3 ± 0.2	7.4 ± 0.5	19.6 ± 0.9	9.2 ± 0.7	21.7 ± 2.6	4.4	75.9	0.02	0.9
6	0.9 ± 0.0	62.0 ± 0.3	3.5 ± 0.5	5.6 ± 0.8	10.6 ± 0.2	7.9 ± 0.1	10.4 ± 1.1	19.9	343.1	0.09	3.1

^{#1} Au/Ti-SiO₂_ALD

^{#2} Au/Ti-SiO2_ALD600.

^{#3} Au/Ti—SiO₂_ALD800.

^{#4} Au/Ti—SiO₂_ALD1000.

^{#5} Au/Ti-SiO₂_IWI.

^{#6} Au/Ti-SiO2_IWI800.

Et: Ethanal; Ac: Acrolein; Pr: Propanal; Ace: Acetone.

a unit: gPO/h·kg_{cat.} Reaction conditions: reaction temperature 200 °C, $H_2/C_3H_6/O_2/N_2 = 3.5/3.5/3.5/24.5$ ml min⁻¹, space velocity = 14,000 ml h⁻¹ g_{cat}-1

b unit: (mmol/h·kg_{cat}).

c turnover frequency, s⁻¹.

cies on the Ti sites increased under reaction conditions because of the increase in the coordination of Ti. [51] In this study, we found that regardless of the preparation method and post-treatment history, the selectivities to propylene oxide, propanal and CO₂ are intrinsically linear functions of the coordination number of Ti as shown in Fig. 8. The selectivity to propylene oxide clearly benefits from low coordination Ti, while high coordination Ti favors high selectivity to propanal and CO₂. The advantage of TiO₂ ALD lies in its ability to generate uniform, site-isolated Ti on SiO₂ which proceeds to form 4-coordinated Ti sites under proper posttreatment. It would have been difficult to achieve the full range from 4-coordinated to 6-coordinated Ti-O if only IWI was used. Higher calcination temperature would possibly further reduce the coordination number of Ti-O, however, the catalysts could be completely inactive in propylene epoxidation due to the melting of the SiO₂ support which was observed at 1200 °C calcination [10]. Our results are in agreement with previous studies [37,40,50]. The hydroperoxide species, which are formed and migrate from Au nanoparticles, must be coordinated first to vacant sites of Ti domains before attacking the propylene double bond to form PO. Without hydroperoxide coordinated on Ti sites, the H₂O formation dominates this process which can decrease the H₂ efficiency. As shown in Fig. 7, the H₂ efficiency improved with the increase in calcination temperature to 800 °C and the decrease in Ti-O coordination number to 4. The tetrahedral Ti sites are also active in the epoxidation of other alkenes such as cyclohexene by t-butyl hydroperoxide (TBHP) or H₂O₂ [52-55]. The structure and reactivity of single site Ti catalysts shown in this work may provide insights into the catalyst performance in other alkenes epoxidation reactions.

3.2. Cluster model of the Ti site

As an approximation, several different cluster models were evaluated as possible structures of the Ti—SiO₂ active site, followed by an analysis of the bond lengths and partial charges on Ti. The simulation of the different coordination sites of Ti—SiO₂ is selected from the nine cluster models listed in Table S3 of the Supporting Information (with optimized configurations shown in Fig. S5). The first two clusters are extracted from the TS-1 structure, and Ti sites are replaced with the Si sites. The middle four clusters come from the unit cell structures of SiO₂ with the Si sites changed to Ti. The bottom three cluster models come from the structure of TiO₂ with the Ti sites replaced with Si sites. In all cases, the Si sites are terminated with hydrogen atoms that are fixed in space to preserve the original lattice structure.

In the DFT calculations, the geometric optimization of the isolated Ti—SiO₂ clusters was performed using the B3LYP functional [56] with 6-31G (d,p) basis set using the Gaussian16[57] package. In order to estimate the partial charge on the Ti site, a natural bond orbital (NBO) analysis[58] was used, with the results listed in Table S3.

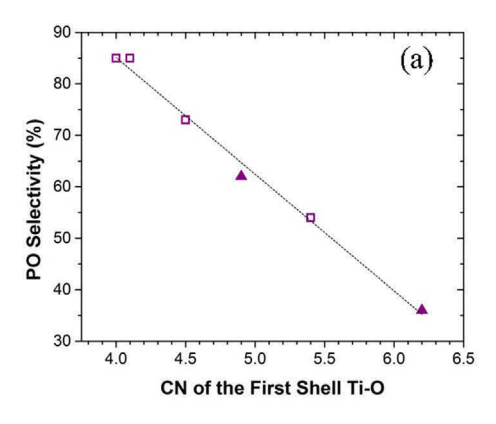
From an analysis of the lowest energy cluster configurations, we found that there is a linear correlation between the Ti charges (Fig. S6) and the Ti—O bond distance ($R_{\text{Ti-O}}$), which is a direct function of the Ti coordination number. When we compared the DFT predictions against the experimental data, we found that (except for the samples of Ti—SiO₂_ALD and Ti—SiO₂_IWI), the coordination number of each sample also has a linear relationship with the bond distance of Ti—O (as shown in Fig. S7).

While we cannot infer any direct information about the reaction mechanism from our DFT cluster calculations, there is a clear relationship between the coordination number, the Ti—O bond distance, and the resulting partial charge on the active Ti site. This level of computational screening may provide useful guidance for tuning and interpreting the catalytic performance of isolated Ti sites in similar environments, and this will be explored more in our future studies.

4. Conclusions

In conclusion, the results presented here show that the selectivity to propylene oxide is linearly correlated to the coordination number of Ti—O in the Ti—SiO₂ support in propylene epoxidation on Au-based catalysts. The single-site, 4-fold coordinated Ti sits favors high PO selectivity and improving hydrogen efficiency, while the single-site, 6-fold coordinated Ti sites prefers the formation of undesired byproducts such as propanal and CO₂. The DFT calculations corroborate the experimental trends in the active site structure and indicate a linear trend in the partial charge of the active site, which might be a useful screening metric for future studies.

The observation of the structure and reactivity of the single site Ti—SiO₂ catalysts are independent of the preparation method but it would have been difficult to establish the full trend without the use of ALD with the uniform isolated sites. The PO selectivity is directly correlated to the coordination number and bond distance of Ti—O. Compared with methods such as IWI, the advantage of ALD lies in its ability to create uniform single site Ti in the initial state, which allows relatively easy manipulation of Ti—O coordination number using lower calcination temperature. By combining ALD, XAS, and DFT, we were able to establish Ti—O coordination number and catalytic properties relationships in a quantitative manner.



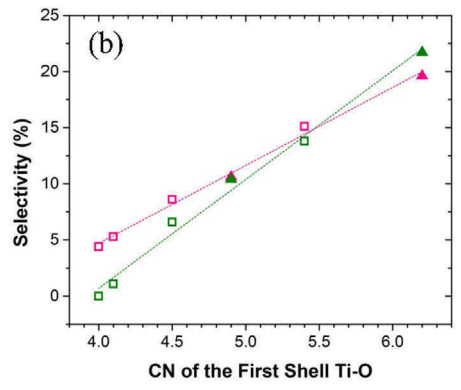


Fig. 8. Selectivity as a function of Ti-O coordination number for (a) propylene oxide and (b) propanal and CO2. Purple - PO; Pink - propanal; Olive - CO2.

Acknowledgements

This work is sponsored by the National Science Foundation (Grant # CBET-1511820 and CBET-1510485). Z. G. gratefully acknowledged the fellowship from the Alabama State funded Graduate Research Scholars Program (GRSP). This research used resources of the Advanced Photon Source, a U.S. Department of Energy (DOE) Office of Science User Facility operated for the DOE Office of Science by Argonne National Laboratory under Contract No. DE-AC02-06CH11357. Computer resources are provided by the Alabama Supercomputer Center.

Appendix A. Supplementary material

Supplementary data to this article can be found online at https://doi.org/10.1016/j.jcat.2019.07.051.

References

- S.J. Khatib, S.T. Oyama, Direct oxidation of propylene to propylene oxide with molecular oxygen: a review, Catal. Rev. 57 (2015) 306–344.
- [2] S. Ghosh, S.S. Acharyya, R. Tiwari, B. Sarkar, R.K. Singha, C. Pendem, T. Sasaki, R. Bal, Selective oxidation of propylene to propylene oxide over silver-supported tungsten oxide nanostructure with molecular oxygen, ACS Catal. 4 (2014) 2169–2174.
- [3] J.L. He, Q.G. Zhai, Q.H. Zhang, W.P. Deng, Y. Wang, Active site and reaction mechanism for the epoxidation of propylene by oxygen over CuOx/SiO2 catalysts with and without Cs+ modification, J. Catal. 299 (2013) 53–66.
- [4] Y.J. Pang, X.H. Chen, C.Z. Xu, Y.J. Lei, K.M. Wei, High catalytic performance of MoO3-Bi2SiO5/SiO2 for the gas-phase epoxidation of propylene by molecular oxygen, ChemCatChem 6 (2014) 876–884.
- [5] Y. Lei, F. Mehmood, S. Lee, J. Greeley, B. Lee, S. Seifert, R.E. Winans, J.W. Elam, R. J. Meyer, P.C. Redfern, D. Teschner, R. Schlogl, M.J. Pellin, L.A. Curtiss, S. Vajda, Increased silver activity for direct propylene epoxidation via subnanometer size effects, Science 328 (2010) 224–228.
- [6] T. Hayashi, K. Tanaka, M. Haruta, Selective vapor-phase epoxidation of propylene over Au/TiO₂ catalysts in the presence of oxygen and hydrogen, J. Catal. 178 (1998) 566–575.
- [7] E.E. Stangland, B. Taylor, R.P. Andres, W.N. Delgass, Direct vapor phase propylene epoxidation over deposition-precipitation gold-titania catalysts in the presence of H₂/O₂: effects of support, neutralizing agent, and pretreatment, J. Phys. Chem. B 109 (2005) 2321–2330.
- [8] T.A. Nijhuis, B.J. Huizinga, M. Makkee, J.A. Moulijn, Direct epoxidation of propene using gold dispersed on TS-1 and other titanium-containing supports, Ind. Eng. Chem. Res. 38 (1999) 884–891.
- [9] T.A. Nijhuis, B.M. Weckhuysen, The direct epoxidation of propene over goldtitania catalysts – a study into the kinetic mechanism and deactivation, Catal. Today 117 (2006) 84–89.
- [10] C.X. Qi, T. Akita, M. Okumura, M. Haruta, Epoxidation of propylene over gold catalysts supported on non-porous silica, Appl. Catal. A 218 (2001) 81–89.
- [11] J. Chen, S.J.A. Halin, E.A. Pidko, M.W.G.M. Verhoeven, D.M. Perez Ferrandez, E.J. M. Hensen, J.C. Schouten, T.A. Nijhuis, Enhancement of catalyst performance in the direct propene epoxidation: a study into gold-titanium synergy, ChemCatChem 5 (2013) 467–478.
- [12] J. Garcia-Aguilar, I. Miguel-Garcia, J. Juan-Juan, Such-Basanez, E. San Fabian, D. Cazorla-Amoros, A. Berenguer-Murica, One step-synthesis of highly dispersed iron species into silica for propylene epoxidation with dioxygen, J. Catal. 338 (2016) 154–167.
- [13] M. Piernavieja-Hermida, Z. Lu, A. White, K.B. Low, T.P. Wu, J.W. Elam, Z.L. Wu, Y. Lei, Towards ALD thin film stabilized single-atom Pd-1 catalysts, Nanoscale 8 (2016) 15348–15356.
- [14] N.C. Cheng, S. Stambula, D. Wang, M.N. Banis, J. Liu, A. Riese, B.W. Xiao, R.Y. Li, T.K. Sham, L.M. Liu, G.A. Botton, X.L. Sun, Platinum single-atom and cluster catalysis of the hydrogen evolution reaction, Nat. Commun. 7 (2016).
- [15] H. Yan, H. Cheng, H. Yi, Y. Lin, T. Yao, C.L. Wang, J.J. Li, S.Q. Wei, J.L. Lu, Single-atom Pd-1/graphene catalyst achieved by atomic layer deposition: remarkable performance in selective hydrogenation of 1,3-butadiene, J. Am. Chem. Soc. 137 (2015) 10484–10487.
- [16] A.T. Bell, B.C. Gates, D. Ray, Basic Research Needs: Catalysis for Energy, in: A.T. Bell, B.C. Gates, D. Ray (Eds.), Report from the U.S. Department of Energy, Basic Energy Science Workshop, U.S. Department of Energy, 2007.
- [17] C.A. Koval, J.A. Lercher, S.L. Scott, Basic Research Needs for Catalysis Science, in: Report of the Basic Research Needs Workshop for Catalysis Science, U.S. Department of Energy, Office of Basic Energy Sciences Workshop, 2017.
- [18] J. Lu, J.W. Elam, P.C. Stair, Atomic layer deposition sequential self-limiting surface reactions for advanced catalyst "bottom-up" synthesis, Surf. Sci. Rep. 71 (2016) 410–472.
- [19] C.P. Canlas, J.L. Lu, N.A. Ray, N.A. Grosso-Giordano, S. Lee, J.W. Elam, R.E. Winans, R.P. Van Duyne, P.C. Stair, J.M. Notestein, Shape-selective sieving layers on an oxide catalyst surface, Nat. Chem. 4 (2012) 1030–1036.

- [20] K. Cho, J.-D. Park, C. Shin, Atomic layer deposition of TiO₂ using titanium isopropoxide and H₂O: operational principle of equipment and parameter setting, J. Semiconduct. Technol. Sci. 16 (2016) 346–351.
- [21] Y. Lei, B. Liu, J. Lu, J.A. Libera, J.P. Greeley, J.W. Elam, Effects of Chlorine in Titanium Oxide on Palladium Atomic Layer Deposition, J. Phys. Chem. C 118 (2014) 22611–22619.
- [22] Z. Lu, M. Piernavieja-Hermida, C.H. Turner, Z. Wu, Y. Lei, Effects of TiO₂ in low temperature propylene epoxidation using gold catalysts, J. Phys. Chem. C 122 (2018) 1688–1698.
- [23] R.M. Almeida, C.G. Pantano, Structural investigation of silica-gel films by infrared-spectroscopy, J. Appl. Phys. 68 (1990) 4225–4232.
- [24] D. Kannaiyan, S.T. Kochuveedu, Y.H. Jang, Y.J. Jang, J.Y. Lee, J. Lee, J. Lee, J. Kim, D.H. Kim, Enhanced photophysical properties of nanopatterned titania nanodots/nanowires upon hybridization with silica via block copolymer templated sol-gel process, Polymers-Basel 2 (2010) 490–504.
- [25] C.H. Huang, H.L. Bai, Y.L. Huang, S.L. Liu, S.I. Yen, Y.S. Tseng, Synthesis of neutral SiO2/TiO2 hydrosol and its application as antireflective self-cleaning thin film, Int. J. Photoenergy (2012).
- [26] S. Rasalingam, R. Peng, R.T. Koodali, Removal of hazardous pollutants from wastewaters: applications of TiO2-SiO2 mixed oxide materials, J Nanomater (2014).
- [27] X.T. Gao, S.R. Bare, J.L.G. Fierro, M.A. Banares, I.E. Wachs, Preparation and insitu spectroscopic characterization of molecularly dispersed titanium oxide on silica, J. Phys. Chem. B 102 (1998) 5653–5666.
- [28] A. Rahtu, M. Ritala, Reaction mechanism studies on titanium isopropoxidewater atomic layer deposition process, Chem. Vap. Deposition 8 (2002) 21–28.
- [29] L.T. Zhuravlev, Concentration of hydroxyl groups on the surface of amorphous silicas, Langmuir 3 (1987) 316–318.
- [30] T. Blasco, M.A. Camblor, A. Corma, J. Perezpariente, The state of Ti in titanoaluminosilicates isomorphous with zeolite-beta, J. Am. Chem. Soc. 115 (1993) 11806–11813.
- [31] F. Geobaldo, S. Bordiga, A. Zecchina, E. Giamello, G. Leofanti, G. Petrini, Drs Uv-Vis and Epr spectroscopy of hydroperoxo and superoxo complexes in titanium silicalite, Catal. Lett. 16 (1992) 109–115.
- [32] J.W. Elam, J.A. Libera, T.H. Huynh, H. Feng, M.J. Pellin, Atomic layer deposition or aluminum oxide in mesoporous silica gel, J. Phys. Chem. C 114 (2010) 17286–17292.
- [33] S. Bordiga, S. Coluccia, C. Lamberti, L. Marchese, A. Zecchina, F. Boscherini, F. Buffa, F. Genoni, G. Leofanti, G. Petrini, G. Vlaic, Xafs study of Ti-silicalite structure of framework Ti(Iv) in the presence and absence of reactive molecules (H2o, Nh3) and comparison with ultraviolet-visible and Ir results, J. Phys. Chem.-Us 98 (1994) 4125–4132.
- [34] F. Babonneau, S. Doeuff, A. Leaustic, C. Sanchez, C. Cartier, M. Verdaguer, Xanes and exafs study of titanium alkoxides, Inorg. Chem. 27 (1988) 3166–3172.
- [35] T. Uozumi, K. Okada, A. Kotani, O. Durmeyer, J.P. Kappler, E. Beaurepaire, J.C. Parlebas, Experimental and theoretical investigation of the pre-peaks at the Ti K-edge absorption-spectra in Tio2, Europhys. Lett. 18 (1992) 85–90.
- [36] F. Farges, G.E. Brown, J.J. Rehr, Ti K-edge XANES studies of Ti coordination and disorder in oxide compounds: comparison between theory and experiment, Phys Rev B 56 (1997) 1809–1819.
- [37] W.S. Lee, C. Akatay, E. Stach, F.H. Ribeiro, W.N. Delgass, Reproducible preparation of Au/TS-1 with high reaction rate for gas phase epoxidation of propylene, J. Catal. 287 (2012) 178–189.
- [38] A.K. Sinha, S. Seelan, S. Tsubota, M. Haruta, Catalysis by gold nanoparticles: epoxidation of propene, Top. Catal. 29 (2004) 95–102.
- [39] J.Q. Lu, X.M. Zhang, J.J. Bravo-Suarez, K.K. Bando, T. Fujitani, S.T. Oyama, Direct propylene epoxidation over/barium-promoted Au/Ti-TUD catalysts with H₂ and O₂: effect of Au particle size, J. Catal. 250 (2007) 350–359.
 [40] X. Chen, S. Chen, A. Jia, J. Lu, W.X. Huang, Gas phase propylene epoxidation
- over Au supported on titanosilicates with different Ti chemical environments, Appl. Surf. Sci. 393 (2017) 11–22.
- [41] T. Liu, P. Hacarlioglu, S.T. Oyama, M.F. Luo, X.R. Pan, J. Lu, Enhanced reactivity of direct propylene epoxidation with H₂ and O₂ over Ge-modified Au/TS-1 catalysts, J. Catal. 267 (2009) 202–206.
- [42] J. Lu, X. Zhang, J.J. Bravo-Suarez, T. Fujitani, S.T. Oyama, Effect of composition and promoters in Au/TS-1 catalysts for direct propylene epoxidation using H₂ and O₂, Catal. Today 147 (2009) 186–195.
- [43] J.H. Huang, E. Lima, T. Akita, A. Guzman, C.X. Qi, T. Takei, M. Haruta, Propene epoxidation with O₂ and H₂: identification of the most active gold clusters, J. Catal. 278 (2011) 8–15.
- [44] D.M.P. Ferrandez, I.H. Fernandez, M.P.G. Teley, M. de Croon, J.C. Schouten, T.A. Nijhuis, Kinetic study of the selective oxidation of propene with O₂ over Au-Ti catalysts in the presence of water, J. Catal. 330 (2015) 396–405.
- [45] X. Feng, N. Sheng, Y.B. Liu, X.B. Chen, D. Chen, C.H. Yang, X.G. Zhou, Simultaneously enhanced stability and selectivity for propene epoxidation with H₂ and O₂ on Au catalysts supported on nano-crystalline mesoporous TS-1, ACS Catal. 7 (2017) 2668–2675.
- [46] T. Ayvali, L. Ye, S. Wu, B.T.W. Lo, C. Huang, B. Yu, G. Cibin, A.I. Kirkland, C. Tang, A.A. Bagabas, S.C.E. Tsang, Mononuclear gold species anchored on TS-1 framework as catalyst precursor for selective epoxidation of propylene, J. Catal. 367 (2018) 229–233.
- [47] B. Taylor, J. Lauterbach, W.N. Delgass, Gas-phase epoxidation of propylene over small gold ensembles on TS-1, Appl. Catal. A 291 (2005) 188–198.
- [48] M. Boudart, Turnover rates in heterogeneous catalysis, Chem. Rev. 95 (1995).
- [49] L.E. Briand, J.M. Jehng, L. Cornaglia, A.M. Hirt, I.E. Wachs, Quantitative determination of the number of surface active sites and the turnover

- frequency for methanol oxidation over bulk metal vanadates, Catal. Today 78 (2003) 257–268.
- [50] G. Mul, A. Zwijnenburg, B. van der Linden, M. Makkee, J.A. Moulijn, Stability and selectivity of Au/TiO2 and Au/TiO2/SiO2 catalysts in propene epoxidation: an in situ FT-IR study, J. Catal. 201 (2001) 128–137.
- [51] J.J. Bravo-Suarez, K.K. Bando, J.I. Lu, M. Haruta, T. Fujitani, S.T. Oyama, Transient technique for identification of true reaction intermediates: Hydroperoxide species in propylene epoxidation on gold/titanosilicate catalysts by X-ray absorption fine structure spectroscopy, J. Phys. Chem. C 112 (2008) 1115–1123.
- [52] H. Kochkar, F. Figueras, Synthesis of hydrophobic TiO2-SiO2 mixed oxides for the epoxidation of cyclohexene, J. Catal. 171 (1997) 420–430.
- [53] C. Beck, T. Mallat, T. Burgi, A. Baiker, Nature of active sites in sol-gel TiO2-SiO2 epoxidation catalysts, J. Catal. 204 (2001) 428-439.
- [54] R.D. Oldroyd, J.M. Thomas, T. Maschmeyer, P.A. MacFaul, D.W. Snelgrove, K.U. Ingold, D.D.M. Wayner, The titanium(iv)-catalyzed epoxidation of alkenes by tert-alkyl hydroperoxides, Angew. Chem. Int. Ed. 35 (1996) 2787–2790.
- [55] G. Sankar, F. Rey, J.M. Thomas, G.N. Greaves, A. Corma, B.R. Dobson, A.J. Dent, Probing active-sites in solid catalysts for the liquid-phase epoxidation of alkenes, J Chem Soc Chem Comm (1994) 2279–2280.
- [56] A.D. Becke, Semiempirical hybrid density functional with perturbative secondorder correlation, J. Chem. Phys. 98 (1993) 5648.
- [57] M. Frisch, G. Trucks, H. Schlegel, G. Scuseria, M. Robb, J. Cheeseman, G. Scalmani, V. Barone, G. Petersson, H. Nakatsuji, Gaussian 16, Revision A. 03, Gaussian, Inc., Wallingford CT, 2016.
- [58] E. Glendening, J. Badenhoop, A. Reed, J. Carpenter, J. Bohmann, C. Morales, F. Weinhold, NBO 5.0, Theoretical Chemistry Institute, University of Wisconsin, Madison, vol. 67, 2001.